THESIS FOR THE DEGREE OF LICENTIATE OF ENGINEERING

Towards Energy-Efficient Drinking Water Production using Biomimicry

SIMON ISAKSSON

Department of Chemistry and Chemical Engineering

CHALMERS UNIVERSITY OF TECHNOLOGY

Gothenburg, Sweden 2017

Towards Energy-Efficient Drinking Water Production using Biomimicry

SIMON ISAKSSON

Licentiatuppsatser vid institutionen för kemi och kemiteknik
Chalmers tekniska högskola
Serial no: 2017:01
ISSN: 1652-943X

Department of Chemistry and Chemical Engineering
Chalmers University of Technology
SE-412 96 Gothenburg
Sweden
Telephone + 46 (0)31-772 1000

Cover:
Illustration showing a proposed water filter design developed with biomimicry in mind. The design comprises mesoporous silica (gray), lipids (brown), and the water-channeling proteins aquaporins (blue). Details on the components of the proposed water filter design are presented in Chapter 2.

Chalmers Reproservice
Gothenburg, Sweden 2017

Towards Energy-Efficient Drinking Water Production using Biomimicry

SIMON ISAKSSON

Department of Chemistry and Chemical Engineering

CHALMERS UNIVERSITY OF TECHNOLOGY

Abstract

Water is a prerequisite for life and we therefore need pure drinking water to survive. Yet there are more than half a billion people that do not have access to pure drinking water. Water treatment can be performed in many different ways, one of the most commonly used being filtration. As the climate is getting warmer and sources of fresh water are being increasingly contaminated, attention is shifted to the sea in the search for drinking water. Sea water does, however, need to be desalinated before it is usable as drinking water.

Desalination is commonly conducted using the process of reverse osmosis (RO), where water is forced to penetrate water-selective barriers in filters. The main issues with reverse osmosis are that the pressure needed to drive the process against the osmotic pressure build-up is significant and that the diffusivity of water through the selectively permeable layer is relatively slow. The energy input needed to run a reverse osmosis process using saline sea water is therefore substantial and the process is mainly performed in large-scale desalination plants. A more energy-efficient solution is needed in order to produce drinking water in a more sustainable manner as well as on a smaller scale.

Nature purifies water in a variety of ways such as large-scale water passage through sand and small-scale purification conducted by mussels. The aim of this thesis was to design a water filter using inspiration from nature. The model system of choice was the water transport across the cell membrane, which is present in both animals and plants. This water transport is conducted by transmembrane proteins called aquaporins, and the aim of this thesis was to incorporate aquaporins in a design that could potentially be used for water filtration purposes.

This thesis proposes a design where aquaporins are supported by mesoporous silica in order to improve robustness. A straightforward assembly process was developed and the resulting design was evaluated using a range of characterization techniques. The results showed that the mesoporous substrate greatly facilitated the spontaneous rupture and bilayer formation from proteoliposomes. Furthermore, neutron reflectivity data provided evidence of protein–silica intercalation where aquaporins made use of the aqueous pore environment to host their extracellular domains. This behavior is thought to improve the robustness of the system. The proposed water filter design put forward in this thesis will hopefully prove useful in the production of drinking water in the future.

Keywords: Water Treatment, Drinking Water, Filter, Biomimicry, Silica, Aquaporin, Membrane Protein, Supported Lipid Bilayer, Liposome

List of publications

This thesis is a summary of the following papers:

I. Protein-Containing Lipid Bilayers Intercalated with Size-Matched Mesoporous Silica Thin Films
Simon Isaksson, Erik B. Watkins, Kathryn L. Browning, Tania Kjellerup Lind, Marité Cárdenas, Kristina Hedfalk, Fredrik Höök and Martin Andersson
Nano Letters, 2016 (Web), DOI: 10.1021/acs.nanolett.6b04493

II. Mesoporous silica nanoparticles with controllable morphology prepared from oil-in-water emulsions
Hanna Gustafsson, Simon Isaksson, Annika Altskär and Krister Holmberg
Journal of Colloid and Interface Science, 2016, 467; 253-260

Contribution report to the listed publications

I. Planned and performed the experimental work and wrote the manuscript.

II. Planned and performed the experimental work together with H.G.

Contents

1 Introduction

Water is commonly considered to be one of the fundamental requirements for life. The Earth is very abundant in water and the water cycle that comprises evaporation, condensation, and precipitation keeps the total amount of water balanced. Despite the abundancy, 663 million people (9 % of the population on Earth) do still not have access to an improved source of drinking water.[1] Access to an improved source of drinking water means access to safe drinking water, whereas lack thereof means less control of the water quality.

1.1 Scarcity of safe drinking water

Although a lot of people do still not have access to an improved source of drinking water, the share of people that do is steadily on the rise. Major improvements were made between 1990 and 2010, when more than 2 billion people gained access to an improved source of drinking water. In 2010, more than 780 million people were however still relying on unsafe drinking water for their everyday needs.[2] Despite the global population growth, this number has continued to decrease steadily to an estimated 748 million in 2012 and 663 million in 2015.[1, 3] Out of these 663 million, 319 million live in sub-Saharan Africa.[1]

The lack of improved drinking water is mainly confined to poorer areas but there are other, more wide spread, drinking water related issues that relate to countries of lower and higher living standards alike. Two of the most pressing drinking water related issues that have rightfully drawn a lot of attention recently are global warming and pollution.

1.1.1 Global warming

A lot of awareness was quite recently raised about the dangers of human-induced global warming. Although more than 90 % of independent climate researchers are of the opinion that the global temperature increase since the start of industrialism is due to human intervention,[4] there are still sceptics that claim the increase to be part of the natural long-term temperature cycle. Regardless of which, temperatures are on the rise with droughts and rising sea levels as results.

The recent drought in California is one example where drinking water supply is limited due to lack of rainfall as a consequence of a drier climate. Another effect of heating is that Arctic ice is melting. This results in rising sea levels, since water that has been withheld in the form of ice melts to water. Large amounts of cold freshly melted water are thereby threatening to weaken the Gulf stream, which could strangely enough lead to a colder climate in the

northern parts of Europe.[5] Another issue with rising sea levels is that cities that are located on the shore are in greater risk of flooding. The saline sea water eventually contaminates ground water that is a common source of drinking water, which means that global warming has a profound impact on water treatment in different ways.

A closely related issue in terms of Swedish drinking water is the situation on Gotland. During the summer in 2016, there was a severe ground water shortage due to a long-term lack of rainfall in the southeastern parts of Sweden. The regional government in Gotland decided to build a desalination plant to convert brackish water of the Baltic sea into drinking water. It was operated during the summer and has the capacity to provide 3000 residents with drinking water, which is 5 % of the population in Gotland. Reverse osmosis (RO) is used to separate the water from ions and other solutes. The required energy for RO in this case is relatively low due to the low salinity of the incoming water and most of the capacity is needed during the tourism-intensive summer period, hence a fair amount of energy can be deduced from solar panels. The drinking water production capacity of the plant is about 20 m^3 h^{-1}.

1.1.2 Pollution

Pollution is a global problem with examples of common pollutants being smog, greenhouse gases and compounds that are toxic to the marine environment. In terms of water pollution, recent concerns regard plastic nanoparticles and pharmaceutical residues. Plastic particles are released from plastics, for instance during washing of clothing made from synthetic fibers. The fibers are mechanically ground into smaller particles that pass through waste water treatment plants and end up in the sea where they are taken up by fish and other animals.[6] Drinking water production is globally often not refined enough to prevent nanoparticles from ending up in the drinking water, which results in human uptake. Another similar example that has recently received a lot of attention is pharmaceutical residues.[7] These are metabolites or degradation products of pharmaceuticals that conduct a similar journey as the plastic particles to end up in our drinking water.

1.2 Water treatment through filtration

There are various ways in which a lack of safe drinking water can be combated, the major and most versatile one being water treatment through filtration. This process is commonly conducted through the use of man-made filters in order to prevent undesired compounds that are larger than the pores in the filter from ending up in the drinking water. Two major types of man-made filters are those based on size exclusion and those based on selective permeability barriers. Since many ions are small species the latter is used in RO, which is the process of converting saline water into drinking water. Saline water is taken from the sea and RO is therefore common in countries that possess a shoreline and have limited access to fresh water, such as Israel and Australia. The selectivity-based permeability barrier is a necessary tradeoff made in order to achieve high purity of the processed water and it usually consists of a phase inversion membrane made from polymers. It has the inherent drawback of fairly low water diffusion rates, hence requiring large amounts of energy to push the water through at decent rates.[8] The specific energy requirement for membrane sea

water desalination is less than 4 kW h m^{-3} whereas the theoretical minimum energy requirement of seawater desalination is 1.29 kW h m^{-3} (at 75 % recovery).[9]

Water treatment is also a common process in nature, where large quantities of water are for instance filtered through sand and gravel in the ground to reach a higher level of purity.

1.2.1 Water filtration inspired by nature

Mankind has copied natural water treatment processes for a long time, with one of the more straightforward examples being the utilization of slow sand filters in waterworks.[10] This kind of approach is typically called biomimicry, an expression coined by Schmitt in 1957. Biomimicry means to mimic biology or nature, using biologically inspired designs or making use of entities derived from nature.[11] There is a range of large-scale biomimetic and bioinspired water treatment solutions available on the market.

In addition to large-scale water treatment, nature performs water filtration on the nanometer scale. This process is conducted across the cell membrane of living cells and it is present in plants as well as animals. The cell membrane consists of many components with lipids being the most abundant, hosting other cell membrane entities in or in connection to a lipid bilayer. An example of a cell membrane entity is the transmembrane protein. Transmembrane proteins are proteins that transverse the cell membrane, some of which are able to act as gateways across the membrane. These gateways are pores that may conduct compound-selective transport of for example calcium ions[12], potassium ions[13] or water[14]. Water-channeling aquaporin proteins are abundant in both plants and animals and one type named aquaporin 4 has been shown to outperform the other aquaporins in water permeability tests.[15] Aquaporins are considered promising in water treatment applications due to their high water selectivity and permeability, a combination of features that phase inversion RO membranes cannot deliver.[8]

The objective of this thesis was to design a proposed water filter using aquaporins with the long-term goal of achieving energy efficient, highly selective and cheap drinking water production. The first design is described in Paper I, which provides a detailed and comprehensive examination of the design, emphasizing the interface between the aquaporins and the porous silica. Paper II describes the production of porous silica nanoparticles with high pore-to-particle diameter ratios. An alternative design to what was presented in article I, using silica particles as the stabilizing layer instead of a film, is currently under consideration.

This thesis consists of 3 major sections: A description of the proposed filter design, an overview of the experimental methodologies and analysis methods used, and a summary of the obtained results.

2

Proposed filter design

In order to produce a water filter using biomimicry, there are a few key components needed. As for any filter, there has to be an impermeable component and a permeable component, which together provide a certain degree of penetration specificity. In the case of selective water transport in and out of the cell the permeable component is the aquaporin. The lipid bilayer is to some extent also water permeable but prevents solutes and other solvents than water from crossing the cell membrane. Aquaporins are transmembrane proteins that facilitate highly specific water transport across the cell membrane.[14] The proposed filter described in this thesis aims at stabilizing aquaporins using straightforward proteoliposome adsorption and rupture on mesoporous silica (Figure 1) in order to potentially achieve energy-efficient and robust drinking water production in the future.

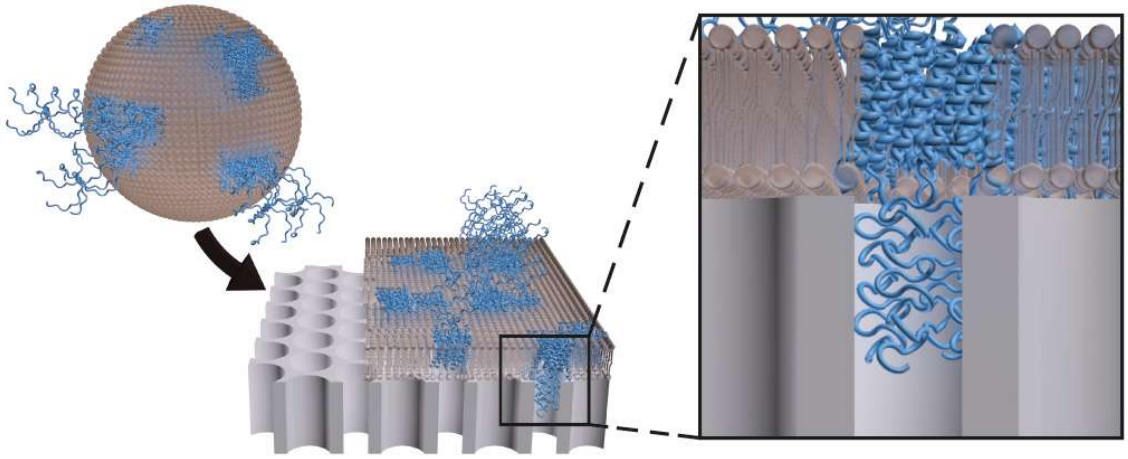

Figure 1. Schematic illustration showing the process of human aquaporin 4 (blue)-containing supported POPC (brown) bilayer formation from proteoliposomes on mesoporous silica (gray). The enlargement depicts extracellular protein domains reaching into a pore in the mesoporous silica.

In Paper I, we have mimicked the cell membrane water transport by incorporating human aquaporin 4 (hAQP4) in a lipid bilayer made of 1-palmitoyl-2-oleoyl-*sn*-glycero-3-phosphocholine (POPC), which is a major constituent of many cell membranes. A free-standing bilayer–aquaporin construct cannot withstand significant forces exerted upon them and since elevated pressures are commonly used to overcome the osmotic pressure differences across desalination membranes, this work utilizes a porous silica film as a mechanical support for the lipid bilayer and the proteins. We developed a layer-by-layer design where the protein-containing supported lipid bilayer (pSLB) is intercalated with the mesoporous silica film. Another way of stabilizing the aquaporins may be to coat porous silica particles with protein-containing lipid bilayers. The silica nanoparticles described in Paper II are suitable candidates that will be evaluated in terms of aquaporin-bilayer intercalation. In order to obtain a filter, the coated particles should be packed into a tight layer through which the aquaporins provide a selective water-permeable pathway.

2.1 Human Aquaporin 4 (hAQP4)

Aquaporins are a group of transmembrane proteins that were first discovered in 1988 by Denker et al.[16] It took another four years until the same group made the discovery that this protein selectively transports water across the cell membrane.[14] Since then, more aquaporins have been discovered in both prokaryotes and eukaryotes. There are 11 mammalian aquaporins known to date (denoted 0-10).[17] Among these there are two subgroups; aquaporins and aquaglyceroporins. Aquaglyceroporins are able to transport small molecules such as glycerol in addition to water whereas aquaporins are exclusively selective for water.

The aquaporin water selectivity is a direct result of the protein structure. Aquaporins are hour-glass shaped transmembrane proteins with 6 alpha-helices fully spanning the cell membrane and two shorter alpha-helices that orient in such a way that they define a part of the pore wall. The ends of the shorter alpha-helices that face the narrow pore are called NPA-motifs since they comprise the amino acid sequence asparagine-proline-alanine (NPA in short). These motifs equip the aquaporin with an electrostatic barrier that blocks the passage of charged species. The water molecules are transported through the aquaporin in a single line, while interacting with carbonyl oxygens in the main chain of the protein. Hydrogen bonds are formed between the water molecules and the carbonyl oxygens, which results in a certain orientation of the water molecules during passage. The aquaporin water selectivity is further enhanced by a selectivity filter, which is located prior to the NPA-motifs. In AQP4, a histidine residue reaches into the channel to restrict the pore diameter to ~1.5 Å.[18]

Human aquaporin 4 (hAQP4) is a 34.8 kDa protein[19] predominantly located in the perivascular end-feet in the brain.[20, 21] It is found in two different splicing isoforms depending on where the splicing mechanism starts. The full-length protein is spliced in such a way that it starts from methionine number 1 (hAQP4M1), whereas the other isoform is spliced so that it starts from methionine number 23 (hAQP4M23). It has been shown that hAQP4M23 is prone to array-formation as opposed to hAQP4M1 that inhibits it.[21]

In this thesis, we have used the hAQP4M23 isoform throughout in order to tailor the underlying substrate according to the defined pattern in which the proteins arrange. The use of the hAQP4M23 isoform as opposed to the hAQP4M1 isoform also favors higher protein-to-lipid ratios due to tighter protein packing through array-formation, which should have a positive impact on the water permeability rate due to the possibility to incorporate more water channels (pores) in the lipid bilayer.

2.2 1-palmitoyl-2-oleoyl-*sn*-glycero-3-phosphocholine (POPC)

Lipids are the main and shape-defining components of membranes present in prokaryotes as well as eukaryotes. They are amphipathic molecules, meaning that they consist of a hydrophilic part and a hydrophobic part. Lipids are commonly pictured as molecules having a head and one or more tails, where the head is the hydrophilic part and the tail is hydrophobic. There are several classes of lipids according to structure. The major class in eukaryotic organisms is glycerophospholipids, comprising phosphatidylcholine, phosphatidylethanolamine, phosphatidylserine, phosphatidylinositol and phosphatidic acid. From these, more than half of the lipids present in eukaryotes are phosphatidylcholines.[22] Furthermore, phosphatidylcholine (PC) is the most abundant class of lipid in mammalian membranes.[23]

One of the most well studied lipids is 1-palmitoyl-2-oleoyl-*sn*-glycero-3-phosphocholine (POPC). It belongs to the phosphatidylcholine lipid class, meaning that it possesses a hydrophobic diacylglycerol backbone carrying a phosphate group, which is esterified to a choline to form the hydrophilic head group.[22] POPC consists of two acyl chains, one saturated and one mono-unsaturated. This structure results in an almost cylindrical shape.[22] Due to their amphipathic character, lipids possess interesting characteristics such as the ability to self-assemble into ordered structures in solution or at interfaces. Their behavior in solution is dependent on the lipid concentration and the properties of the solvent. When the concentration of lipids in aqueous solution reaches the critical micelle concentration (CMC) the lipids start to form micelles in which their hydrophobic tails are oriented towards the center and the hydrophilic heads towards the solution. At higher concentrations the lipids arrange into bilayer structures adopting for example spherical shapes, as in the case of the vesicles used in this thesis. One way of studying lipid bilayers in more detail is to deposit them on a surface, which was done in this thesis. The resulting structure is a supported lipid bilayer (SLB), which is more robust than a non-supported bilayer and convenient to investigate in detail due to its flat geometry.

2.3 Mesoporous silica

Silica (SiO_2) is an amorphous material that is abundant in sand and used as the main constituent in glass. It is widely used in industrial applications in the form of colloidal particles, which have traditionally been produced using the established Stöber process.[24]

Mesoporous silica particles, by definition having pore diameters of 2-50 nm,[25, 26] were first presented by researchers at the Mobil corporation in 1992 using surfactants (surface active agents) as pore templating agents.[27] In 1998, Zhao *et al.* produced mesoporous particles with larger pores using block-copolymers as templating agents instead of surfactants.[28] Surfactants and the block-copolymers used by Zhao *et al.* are similar in the sense that both

are amphipathic. Surfactants and amphipathic block-copolymers do therefore self-assemble into well-defined structures when dispersed in solution. What structure the amphipathic molecules form is mainly governed by the entropy. Intermolecular forces between surfactants as well as between surfactants and water play a major role in the strive to achieve an as low-as-possible energy state of the system.

At high surfactant concentrations the self-assembly results in long-range ordered liquid crystalline phases that arrange in for example lamellar, cubic or hexagonal structures. These liquid crystalline structures can be used for pore templating of silica nanoparticles. In order to form silica from the liquid crystalline mold, a silica precursor molecule is used. Commonly used precursors are silicon alkoxides, which hydrolyze in the presence of water according to

$$\equiv Si - OR + H_2O \leftrightarrow \equiv Si - OH + ROH \quad (1)$$

where the three stacked horizontal lines depict the covalent bonds between silicon and the additional alkoxide groups of the precursor. The hydrolysis results in the formation of silanol groups (Si-OH), that starts a condensation polymerization reaction according to

$$\equiv Si - OR + HO - Si \equiv \leftrightarrow \equiv Si - O - Si \equiv \ + ROH \quad (2)$$

$$\equiv Si - OH + HO - Si \equiv \leftrightarrow \equiv Si - O - Si \equiv \ + H_2O \quad (3)$$

The formed ≡Si–O–Si≡ linkages are called siloxane bridges and they are the backbone of silica. In addition to siloxane bridges there are also silanol groups present, in particular on the silica surface. These are more reactive than the siloxane bridges and can therefore be used for functionalization purposes.

The same concept of silica precursor hydrolysis followed by condensation can be used to form mesoporous silica thin films. A very convenient methodology to form mesoporous silica thin films was presented by Brinker *et al.*[29] They introduced the evaporation-induced self-assembly (EISA) process, in which a volatile solvent is added to the reaction mixture. The volatile solvent will evaporate quickly upon deposition onto a substrate, which can be performed using methods such as spin-coating or dip-coating. Rapid solvent evaporation leads to the formation of liquid crystalline structures in the non-volatile solvent remaining on the substrate, in which the silica precursor hydrolysis and condensation reactions take place to form mesoporous silica.[29] The silicon alkoxide used as a precursor in this thesis was exclusively tetraethylorthosilicate (TEOS).

3

Experimental

The experimental procedures utilized in this thesis relate to the design of the proposed biomimetic water filter. This section starts by providing an overview of the preparation methods followed by a description of the analysis techniques used to produce and characterize the proposed filter. Both the section on preparation methods and the section on analysis techniques are ordered in a top to bottom fashion; starting with the mesoporous silica support before moving into proteoliposome preparation and finishing with the proposed filter design.

3.1 Preparation methods

The preparation methods used in this thesis are presented according to the proposed filter design, moving from the mesoporous silica substrates into protein production and proteoliposome incorporation before reaching pSLB formation.

3.1.1 Mesoporous silica thin films

Mesoporous silica films were formed using the nonionic block copolymer poly(ethylene glycol)$_{20}$-poly(propylene glycol)$_{70}$-poly(ethylene glycol)$_{20}$ (Pluronic P123) as templating agent. In P123 the centrally positioned hydrophobic poly(propylene glycol) chain folds to orient the hydrophilic poly(ethylene glycol) chains in the same direction, which gives rise to the amphipathic behavior.[26] The silicon alkoxide TEOS was used as the silica precursor. The EISA method was used to prepare mesoporous silica thin films on glass substrates, QCM-D crystals, titanium discs, and silicon blocks. Briefly, pre-hydrolysis of TEOS was conducted by mixing TEOS, EtOH and HCl (pH 2). P123 was meanwhile dissolved in EtOH and then mixed with the pre-hydrolyzed TEOS solution. The solution was deposited onto substrates using spin-coating. The rapid evaporation of EtOH during the spin coating process induced liquid crystalline phase formation in the remaining aqueous phase containing P123. The pre-hydrolyzed TEOS continued to hydrolyze in the presence of water and the low pH catalyzed the reaction. The resulting silanol species condensed and polymerized into silica, which was formed in accordance to the liquid crystalline phase imposed by P123. Mesoporous silica was obtained by heat treatment in which the organic P123 was burnt off to leave pores within the amorphous silica film.

3.1.2 Mesoporous silica particles

Mesoporous silica particles with a high pore to particle diameter ratio and potentially similar pore diameters as for the mesoporous silica thin films were formed and characterized. We were interested in the Hiroshima mesoporous material (HMM) particle synthesis developed

by Nandiyanto *et al.* in 2009,[30] since HMM particles possess some of the desired characteristics. The original particle synthesis protocol did, however, seem unusually complex. In order to simplify the synthesis process, the polymer, the polymerization initiator and the inert atmosphere were removed from the synthesis procedure. In addition, the proposed catalyst L-lysine was substituted for ethanolamine in 3 out of the 4 synthesis procedures. The particle size and pore morphology were optimized using 3 different surfactants as templating agents, in addition to CTAB that was used in the original synthesis (Figure 2). Particles synthesized using CTAB were denoted MPS-1, whereas particles synthesized using 12-6-12, 12-2-12, and Ethylan 1008 were denoted MPS-3, MPS-4, and MPS-5, respectively. The formation of a water-in-oil-in-water (W/O/W) double emulsion was conducted by vigorous mixing of surfactant, de-ionized water, n-octane and L-lysine/ethanolamine at 70 °C. TEOS was added to the emulsion, entering the oil phase due to the alkoxide hydrophobicity. TEOS hydrolysis was initiated at oil–water interfaces, followed by silica condensation. The reaction was continued for 20 h, after which the reaction mixture was decanted into a separation funnel. The water phase was collected and freeze dried in order to retrieve the particles, which were then heat-treated to remove the pore-templating surfactants.

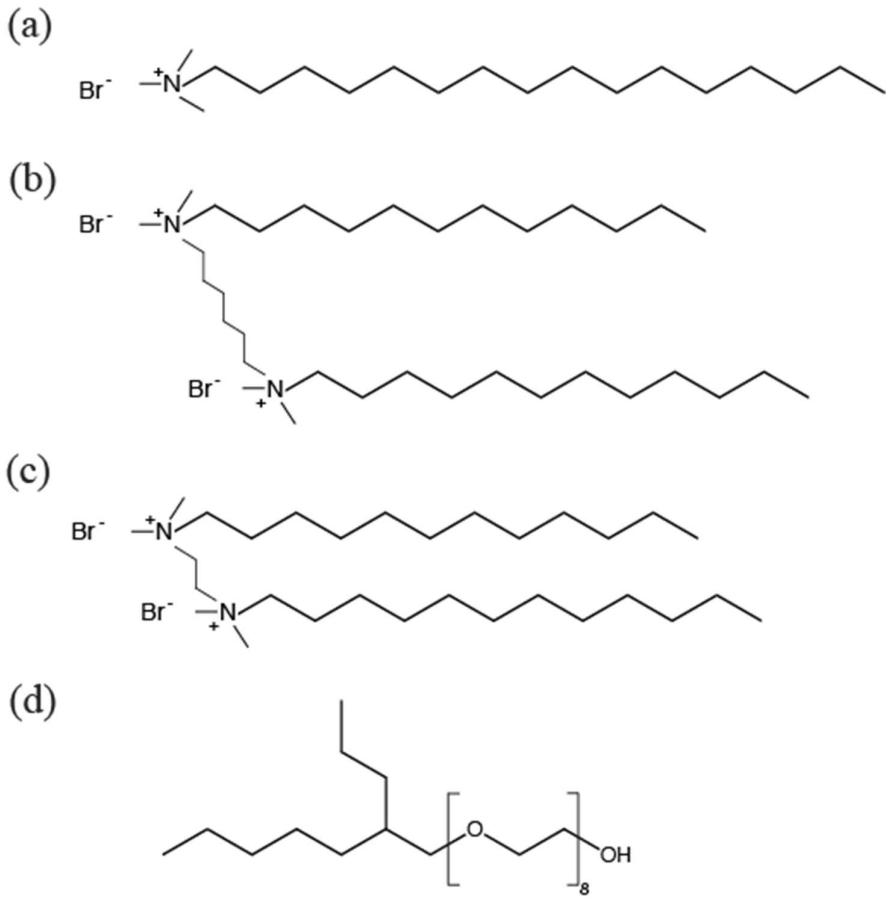

Figure 2: Chemical structure of (a) the cationic surfactant CTAB, (b) the cationic gemini surfactant 12-6-12, (c) the cationic gemini surfactant 12-2-12, and (d) the nonionic surfactant Ethylan 1008.

3.1.3 hAQP4 protein production

hAQP4 transmembrane proteins were recombinantly overexpressed in *Pichia pastoris* yeast cells, followed by cell membrane breakage and protein purification. Briefly, the gene coding for hAQP4 was amplified using the polymerase chain reaction (PCR) and cloned into the *P. pastoris* vector pPICZB together with a sequence coding for a C-terminal hexa-histidine tag. *P. pastoris* cells containing the pPICZB vector were selected in a zeocin screening process. The constructs were linearized and transformed into wild-type *P. pastoris* using the lithium chloride method, where the cells were resuspended in LiCl and subjected to heat shock in order for the cell membrane to become permeable to DNA. The transformed cells were grown in a bioreactor after which the cell membranes were subjected to breakage in a French pressure cell press, washed, and solubilized. The solubilized material was collected through centrifugation and from this material, hAQP4 was singled out in a Ni-NTA column that selectively targeted the His-tag on the C-terminal protein domain. The purified proteins were stabilized in *n*-octyl-β-D-glucoside (β-OG) until proteoliposome incorporation.

3.1.4 Proteoliposome preparation

Proteoliposomes were formed by incorporation of purified hAQP4 into liposomes made of zwitterionic POPC. Briefly, POPC was dissolved in chloroform upon delivery and subjected to rotary evaporation to form a lipid film. The lipid film was resuspended in Tris buffer to yield multilamellar POPC liposomes, which were formed through the process of molecular self-assembly. hAQP4 was incorporated into the lipid bilayer of the liposomes through a reconstitution process. Briefly, liposomes were mixed with extra Tris buffer constituents and partly solubilized in β-OG detergent. Detergent-stabilized hAQP4 was added to the mixture, whereby Biobeads SM2 adsorbent was added to withdraw β-OG. As the detergent was removed, the proteins spontaneously inserted into the liposome bilayer since they were no longer detergent stabilized in solution. Biobeads were removed by decantation and the proteoliposomes were subject to spin column filter centrifugation to produce unilamellar proteoliposomes having a certain size distribution.

3.1.5 Protein-containing supported lipid bilayer formation

pSLB formation is a matter of spontaneous proteoliposome adsorption, fusion and rupture on the mesoporous silica substrate. This process was straightforward both using a continuously flowing proteoliposome solution and without using any flow at all. Briefly, proteoliposomes in Tris buffer were deposited onto a mesoporous silica substrate. Proteoliposome diffusion and interaction with the negatively charged silica (pH 8) resulted in spontaneous proteoliposome adsorption on the mesoporous silica surface. Continuous adsorption led to crowding of proteoliposomes on the surface, resulting in proteoliposome–proteoliposome interactions. These interactions in combination with the proteoliposome–silica interactions eventually led to proteoliposome fusion and rupture, which finally resulted in pSLB formation.

3.2 Analytical techniques

Characterization of organic and inorganic matter as well as the interface between them requires the use of a range of analytical techniques. This section describes the analytical techniques utilized in this thesis.

3.2.1 Silica characterization

Mesoporous silica is the inorganic component of the proposed water filter design. It is not as sensitive to harsh environments as the organic components and was therefore studied using electron microscopy (SEM, TEM) and SAXS.

3.2.1.1 Electron microscopy

Electron microscopy was employed to characterize the pore ordering and morphology of mesoporous silica thin films and particles.

3.2.1.1.1 Scanning electron microscopy (SEM)

SEM is a non-destructive analysis technique operated in an ultra-high vacuum environment. The sample is scanned by an electron beam, which results in the emission of secondary and back-scattered electrons from the sample surface. These are detected to provide information on the surface morphology and surface composition of the sample.

The acceleration voltage for the electrons in the electron beam can be adjusted to tune the performance of the analysis according to the sample material. Silica is a bad conductor, which means that the electrons from the electron beam accumulate in the sample without adequate escape routes. The introduction of charge effects is undesired and can partially be avoided by lowering the acceleration voltage. Lowering the acceleration voltage decreases the electron penetration depth and hence the detection depth. In this thesis, SEM analysis on mesoporous silica samples was commonly conducted in the range of 2-5 kV using a Leo Ultra 55 FEG SEM (Zeiss).

3.2.1.1.2 Transmission electron microscopy (TEM)

TEM analysis is operated using an electron beam in ultra-high vacuum conditions. Higher acceleration voltages are used compared to SEM in order to allow the electrons to pass through thin samples. Electrons are scattered on their way through the sample and the magnitude of scattering is dependent on the density and thickness of the material. The scattering is monitored by focusing the transmitted electrons onto a fluorescent screen. A dense material hinders the passage of electrons, resulting in a dark projection.

In this thesis, TEM analysis of mesoporous silica films and particles was performed using a JEM-1200 EX II (JEOL) operated at 120 kV acceleration voltage. Thin particle slices embedded in epoxy were analyzed using a LEO 706E operated at 80 kV acceleration voltage. TEM analyses provided data on the porous structure inside the material in addition to the surface.

3.2.1.2 Small-angle X-ray scattering (SAXS)

SAXS was used to study long-range pore ordering in mesoporous silica. X-rays have a wavelength on the order of lattice planes in crystalline materials and are therefore suitable for studying mesoporous materials with repetitive long-range ordered porosity. The sample is exposed to a high intensity X-ray beam which hits the sample at a low angle (<10°), whereby radiation is scattered upon interaction with the electrons in the material. The intensity of the scattered radiation is plotted as a function of the scattering angle 2θ or the momentum transfer q. SAXS studies of long-range ordered materials result in diffractogram Bragg peaks due to constructive interference of scattered radiation. The relation between Bragg peaks was used to determine the long-range porous ordering in the material.

Silica has a relatively high electron density, which results in fairly good scattering of X-rays. In order to improve the signal further, a radiation source providing a high flux of photons is used. One such source is the synchrotron facility MAX-lab in Lund, where the SAXS analyses in this thesis were performed (beamline I911).

3.2.1.3 N_2 physisorption

N_2 physisorption was used to assess the specific surface area, pore size, and pore size distribution of the mesoporous silica particles. Interactions between N_2 and the silica surface are probed by controlled filling of empty pores in the particles, hence the first step was to degas the sample. The temperature was also lowered to 77 K prior to N_2 addition. First, a monolayer of nitrogen was produced on the surface of the silica by increasing the N_2 pressure. The monolayer data was processed using the universal gas law and the Brunauer–Emmet–Teller (BET) method to quantify the amount of adsorbed nitrogen.[31] By increasing the N_2 pressure further the pore size and shape can be assessed. The N_2 pressure was increased until the onset of N_2 condensation (pore saturation), followed by a pressure decrease which resulted in N_2 evaporation. The Barrett–Joyner–Halenda (BJH) method was used to calculate the pore size.[32]

N_2 physisorption measurements were conducted using a Micromeritics ASAP 2010 instrument.

3.2.2 Proteoliposome characterization

Characterization of proteoliposomes prior to pSLB formation was performed using electron microscopy and light scattering.

3.2.2.1 Cryogenic Transmission electron microscopy (cryo-TEM)

Cryo-TEM is a version of TEM (presented above) that can be used to study organic samples. As previously stated, TEM uses ultra-high vacuum conditions and high electron beam acceleration voltages to provide high-resolution data on the material composition of thin samples. The harsh analysis conditions in the TEM cannot be used to study biological samples. In cryo-TEM, the sample is rapidly frozen and embedded in amorphous ice in order to be analyzed in TEM. Rapid plunge-freezing of the sample is critical in order to prevent formation of ice crystals that can disrupt the sample structures. The sample was

therefore plunged into liquid ethane (–180 °C) and transferred to a sample stage which was cooled by liquid nitrogen through the duration of the analysis.

Cryo-TEM analysis was performed using a Philips CM120 cryo-TEM operated at 120 kV acceleration voltage.

3.2.2.2 Light scattering

Light scattering is essentially a mechanism of adsorption and re-emission of electromagnetic radiation.[33] The incoming electromagnetic wave interacts with matter by setting electrons and protons into oscillatory motion. Analysis techniques based on light scattering were in this thesis utilized to determine proteoliposome size and to probe hAQP4 water transport capabilities.

3.2.2.2.1 Dynamic light scattering (DLS)

Dynamic light scattering (DLS), also known as photon correlation spectroscopy (PCS) or quasi-elastic light scattering (QELS), was used to assess the size distribution of proteoliposomes. In DLS, the sample is irradiated by monochromatic light, which is either absorbed or scattered by the sample. Scattered light is monitored and the scattering angle in relation to the incoming light is determined.[33] In dispersed particle systems as proteoliposomes in buffer, the main contribution to the scattering signal is caused by differences in refractive indices between the proteoliposomes and the surrounding buffer.

Time-resolved light scattering measurements are employed to probe the movement of the scattering entities due to diffusion. Relaxation times can be determined from the diffusion characteristics of a sample, which in turn can be used to calculate the size of the scattering entities.

A Malvern Zetasizer Nano ZS that was operated at a fixed angle of 173° was used for the DLS measurements presented in this thesis.

3.2.2.2.2 Stopped-flow light scattering

Stopped-flow light scattering was used to assess the water transport capabilities of hAQP4. In stopped-flow light scattering, sub-second kinetics of systems can be assessed upon rapid mixing of reactants. Upon mixing, the flow is stopped and the transition from reactants into the resulting compound sample is monitored using light scattering.

In order to assess hAQP4 water transport capabilities, the proteoliposome solution was mixed with a hyperosmolar solution containing sucrose. The rapid introduction of sucrose in the proteoliposome surroundings upon mixing results in an osmotic gradient. The osmotic gradient results in water transport out of the proteoliposomes in order to dilute the sucrose and thereby balance the concentration of osmolytes across the bilayer. The rapid proteoliposome shrinkage is detected as changes in scattered light as a function of time, which can be fitted to an exponential function on the form

$$I = A_1 e^{-k_1(t-t_0)} + A_2 e^{-k_2(t-t_0)} + A_3 \quad (4)$$

where I is the measured intensity, A_1, A_2, and A_3 are coefficients, k_1 and k_2 are rate constants, t is the time, and t_0 is the starting time. The rate constants of shrinkage can then be used to calculate the osmotic water permeability P_f from

$$P_f = \frac{k}{(S/V_0) \cdot V_w \cdot c_{out}} \quad (5)$$

where S/V_0 is the ratio of external surface area to internal volume, V_w is the partial molar volume of water, and c_{out} is the external osmolality.[34]

The stopped-flow light scattering equipment used in this thesis was an SFM 2000 (BioLogic Science Instruments) operated at a fixed 90° detection angle.

3.2.3 Protein-containing supported lipid bilayer (pSLB) characterization

The pSLB formation process and the proposed filter design were studied using surface sensitive techniques and neutron reflectivity. The use of these analysis methods allows verification of the existence of the proposed filter design and to study the interaction between the mesoporous silica and the pSLB.

3.2.3.1 Surface sensitive techniques

Surface sensitive techniques provide detailed information on a few surface layers of a material. In this thesis, surface sensitive techniques were employed to study the final step in the proposed filter design, i.e. pSLB formation.

3.2.3.1.1 Quartz crystal microbalance with dissipation monitoring (QCM-D)

Quartz crystal microbalance with dissipation monitoring (QCM-D) was employed to study the pSLB formation process. QCM-D is a surface sensitive technique that analyzes the mass deposition onto a surface as a function of time. The surface of interest is applied on a quartz crystal with two gold electrodes. An AC voltage is applied across the crystal, resulting in crystal oscillation in a shearing mode. The crystal oscillates at its acoustic resonance frequency, which is altered when mass is deposited on the surface. Mass adsorption results in a negative frequency shift. Provided that the deposited matter is rigid, the obtained frequency can be converted into mass using the Sauerbrey relation

$$\Delta m = -\frac{\Delta f \times C}{n} \quad (6)$$

where Δm is the adsorbed mass, Δf is the frequency shift, C is the mass sensitivity constant (17.7 ng Hz^{-1} cm^{-2}), and n is the overtone number. In addition to the deposited mass, QCM-D also assesses the viscoelastic properties of the adsorbent by monitoring the dampening in the system upon deposition.

The QCM-D results presented in this thesis were obtained using a QCM-D E4 system coupled to a peristaltic pump.

3.2.3.1.2 Total internal reflection fluorescence (TIRF) microscopy

Total internal reflection fluorescence (TIRF) microscopy was used as a complementary method to QCM-D for studying the pSLB formation process. TIRF microscopy is a branch of fluorescence microscopy, which in turn is a subset within optical microscopy. Optical microscopy uses visible light to image objects using optics for magnification. The limitation of optical microscopy is the diffraction barrier using visible light, which resides at approximately half the wavelength of the light used to image the object. The pSLB presented in this thesis consists of lipids and proteins that are smaller than the diffraction barrier and cannot therefore be imaged using regular optical microscopy.

Fluorescence microscopy is a means of imaging small entities using optical microscopy. The lipids and proteins used in this thesis are not inherently fluorescent and therefore need to be labeled with a fluorescent dye. A fluorescent dye is a molecule that has the ability to excite electrons to a higher energy level by absorbing incoming photons of energies matching the band gap between the excited state and the ground state. The excited state is however not stable and excited electrons are forced into a lower and more stable energy state in the process of relaxation. The electrons do not always go back to the ground state but rather to an intermediate state, meaning a smaller energy gap and hence a longer wavelength compared to that used to excite the electron in the first place. The benefit of this is that the specific fluorescence wavelength can be isolated from the illumination wavelengths using filters. This results in specific detection of fluorescent molecules.

TIRF microscopy is a method used to specifically image fluorescent entities close to a surface and is hence beneficial in the study of substrate-supported planar membranes.[35] An evanescent field is created from the interface between a substrate surface and a liquid when the angle of incidence of the incoming light is larger than the critical angle, which results in total reflection at the interface. The evanescent field decays exponentially with the distance from the surface in the direction perpendicular to the surface. Hence, the evanescent field only reaches a couple of 100 of nanometers into the bulk, making it a good method for probing surface interactions.

The TIRF microscopy setup used in this thesis was inverted, meaning that the substrate–liquid interface was imaged from below, through the transparent glass substrate. A Nikon Eclipse Ti-E microscope equipped with an Andor Ixon+ camera and a 60× oil immersion objective was used.

3.2.3.1.2.1 Fluorescence recovery after photobleaching (FRAP)

Fluorescence recovery after photobleaching (FRAP) was used to assess the fluidity of lipids and proteins in the pSLB. In the FRAP[36, 37] analyses conducted in this thesis, TIRF microscopy (presented above) was used to image movement of the fluorescent entities after disrupting their fluorescence in a specific area using a high intensity laser. The lipids located in the bleached area will diffuse out of that area whereas fluorescent lipids will diffuse into the bleached spot, homogenizing the lipid bilayer. This process was monitored through time lapse imaging from which a diffusion coefficient was calculated.

3.2.3.2 Neutron reflectivity (NR)

Neutron reflectivity (NR) was used to study the organic–inorganic interface in detail. Neutrons have wavelengths on the order of atomic distances, allowing them to provide highly resolved material data. Since they are not charged, they do not interact electrostatically with protons and electrons, allowing neutrons to non-destructively penetrate deep into materials.

In the study of the proposed filter design presented in this thesis, neutrons were approaching the sample through a single-crystal silicon block. Every material has its neutron refractive index called a scattering length density. Neutrons thereby get reflected by an angle θ at the interface to a material having a higher scattering length density. Since neutrons interact with atomic nuclei the analysis is sensitive to isotopic differences as for instance the difference between hydrogen and deuterium. Isotopic substitution can therefore be used to increase the contrast between the entity of interest and the surroundings. In this thesis, H_2O was substituted for D_2O to enhance the contrast.

The NR experiments presented in this thesis were conducted at the SURF reflectometer at ISIS, STFC Rutherford Appleton Laboratory (Didcot, UK).[38] At this site, neutrons are produced through spallation. Spallation involves firing high-energy protons into a tungsten target, which induces a nuclear reaction that produces neutron beams.

4

Results and Discussion

In this section, results obtained during the design of the proposed filter structure are presented. The chapter is divided into sections according to the proposed filter design, starting from the mesoporous silica to eventually move into pSLB characterization.

4.1 Mesoporous silica thin films

Structural and morphological characterization of mesoporous silica thin films was conducted using TEM, SEM and SAXS (Figure 3). The mesoporous film had an ordered porous structure as shown by TEM (Figure 3A) and SAXS (Figure 3B). The q-ratios between the peaks in the SAXS diffractogram revealed that the pores were hexagonally ordered, which was confirmed by TEM. The pore diameter of the material was uniform at ~6 nm, as shown by TEM and SEM (Figure 3C). The pore visibility in SEM also revealed that the pore network was accessible from the surface of the film. Cross-section SEM was employed to assess the film thickness, which proved to be ~300 nm (Figure 3D).

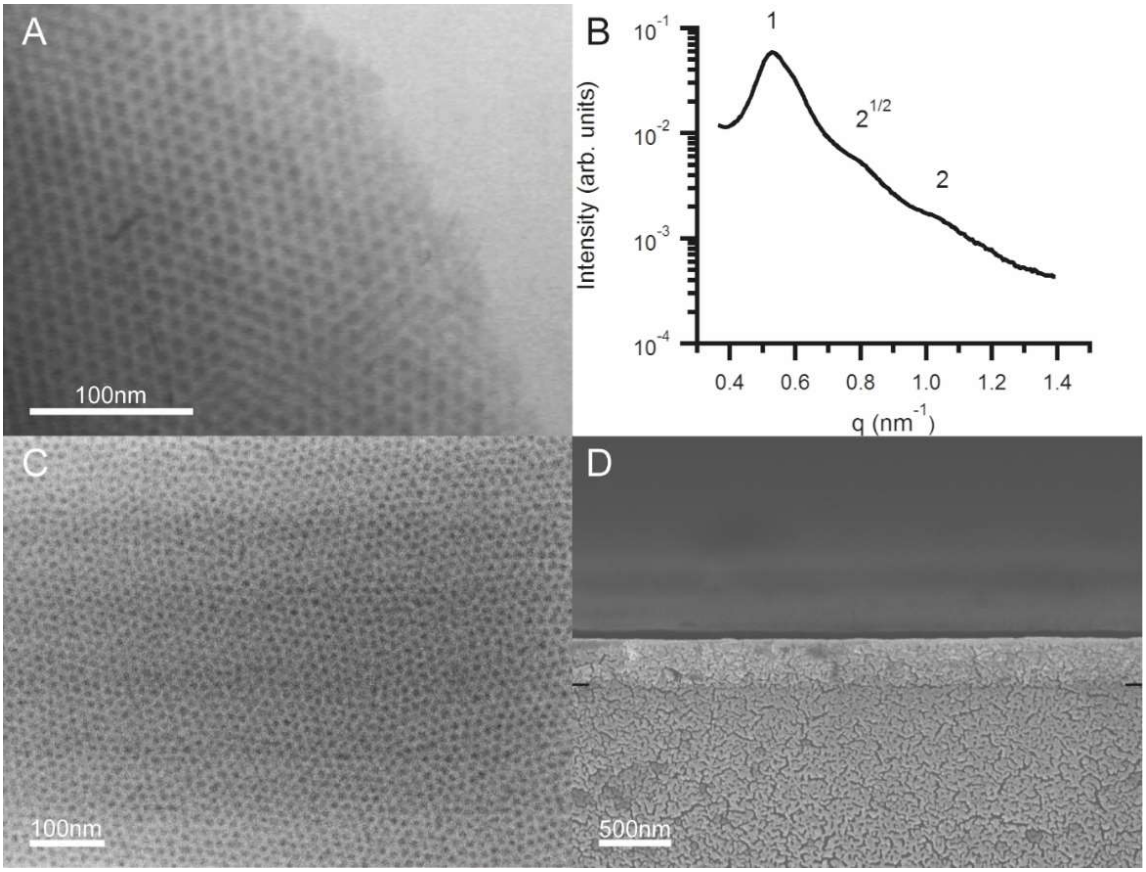

Figure 3. (A) TEM micrograph showing hexagonal ordering of the porous network in the mesoporous silica substrate. The pores are uniform with a diameter of 6 nm. (B) SAXS data providing evidence of long-range hexagonal pore ordering in the mesoporous silica substrate. The numbers above the Bragg peaks denote the relative q-ratios between the peaks. (C) Top view of the mesoporous silica surface captured by SEM. Pores with pore diameters of ~6 nm are accessible from the surface. (D) SEM cross section of mesoporous silica thin film deposited on a glass slide (silica–glass interface is depicted by black lines). The mesoporous thin film is ~300 nm thick.

4.2 Mesoporous silica particles

Structural and morphological characterization of mesoporous silica particles was conducted using TEM, SEM and N_2 physisorption. TEM micrographs (Figure 4) show elongated pores for all four types of particles synthesized using the surfactants cetyltrimethylammonium bromide (CTAB, Figure 4A), 12-6-12 (Figure 4B), 12-2-12 (Figure 4C), and Ethylan 1008 (Figure 4D), respectively. Particles templated using CTAB and 12-2-12 clearly showed wider pores than the other two particle types.

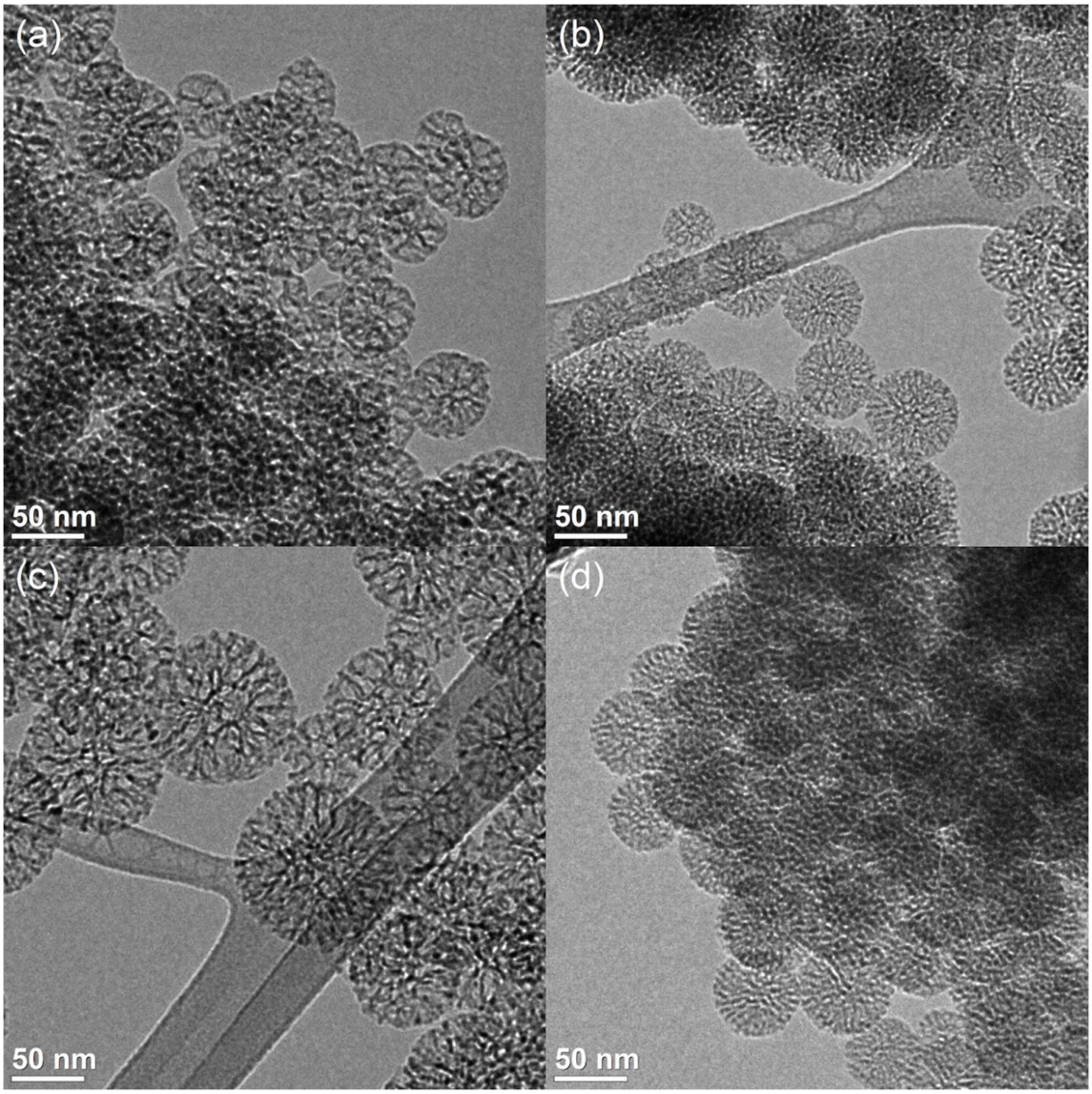

Figure 4. TEM micrographs of (a) MPS-1 (CTAB), (b) MPS-3 (12-6-12), (c) MPS-4 (12-2-12), and (d) MPS-5 (Ethylan 1008).

SEM micrographs (Figure 5) of the same four particle types clearly show elongated pores on the surface of particles templated using CTAB (Figure 5A) and 12-2-12 (Figure 5C). The pores are hardly distinguishable on particles synthesized using 12-6-12 (Figure 5B) and Ethylan 1008 (Figure 5D) as pore templating agents, which correlates well with TEM data (Figure 4) showing wider pores for MPS-1 and MPS-4. The data provided by SEM concluded that MPS-1 and MPS-4 possessed pores that were accessible from the particle surface, whereas the pore accessibility of MPS-3 and MPS-5 was more difficult to assess due to the narrower pore width of these materials.

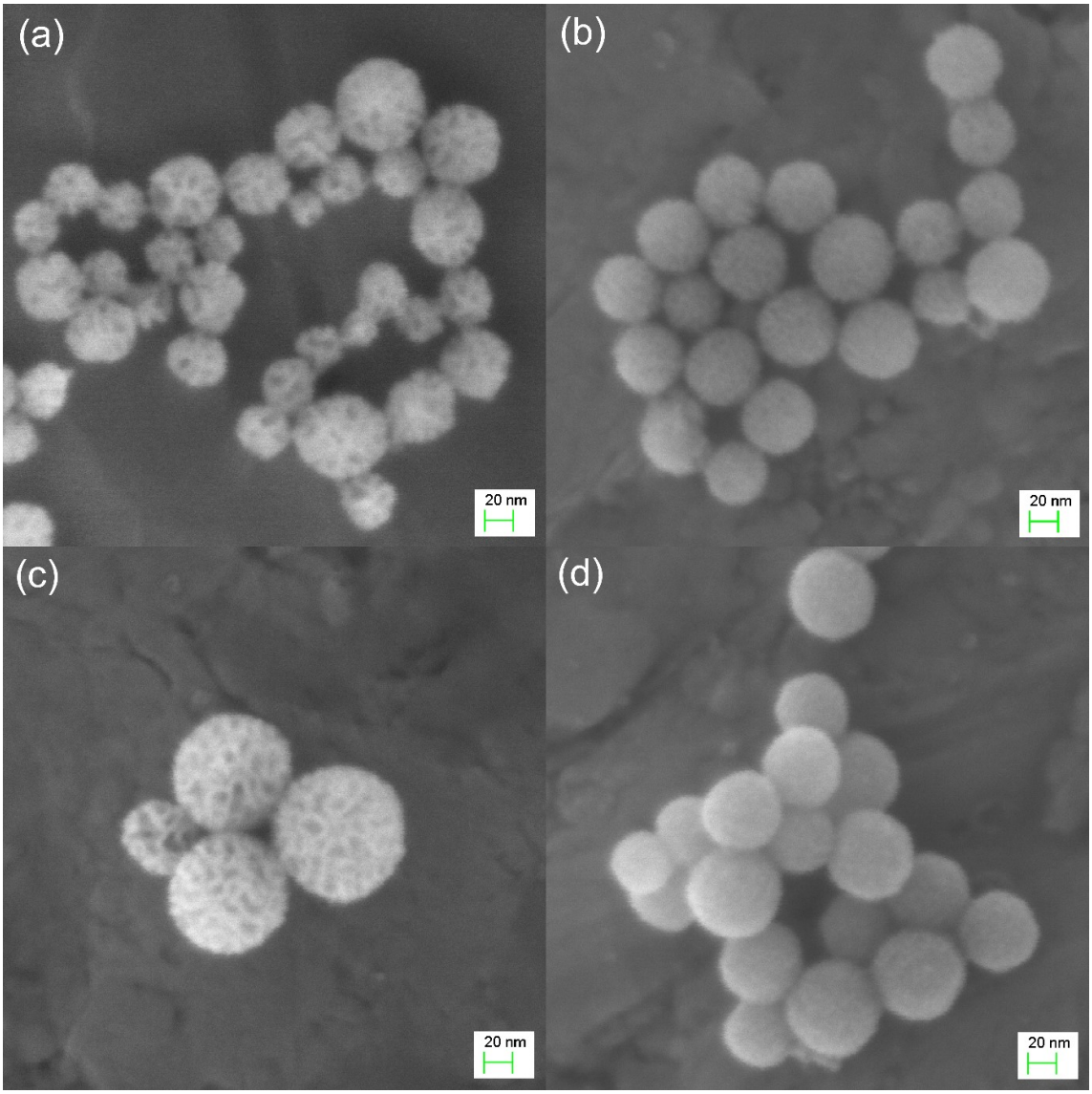

Figure 5. SEM micrographs of (a) MPS-1 (CTAB), (b) MPS-3 (12-6-12), (c) MPS-4 (12-2-12), and (d) MPS-5 (Ethylan 1008).

Mean particle diameters calculated based on a minimum of 25 particles from TEM and SEM micrographs are presented in Table 1. The results showed that the particle diameter ranged between 53 nm (MPS-1) and 91 nm (MPS-4), with all samples showing a similar degree of polydispersity.

Table 1. Mean particle sizes as determined from SEM and TEM.

Material	Mean particle diameter (nm)	Number of analyzed particles	Standard deviation (% of mean value)
MPS-1	53	25	16
MPS-3	56	25	12
MPS-4	91	30	14
MPS-5	60	25	11

The pore width and particle morphology was investigated in more detail using N_2 physisorption (Figure 6). The adsorption–desorption isotherms showed Type IV behavior for all of the particles (Figure 6A), which is typical for mesoporous materials.[39] Table 2 shows the BET surface areas and the total pore volume within the particles. All particles showed values within the range of mesoporous materials. MPS-3 and MPS-5 showed higher BET surface area per unit of mass than MPS-1 and MPS-4, which is in accordance with the differences in pore widths that were seen from TEM and SEM since smaller pore diameters mean higher surface area to pore volume ratios. Smaller pores do therefore frequently result in higher BET surface area per unit of mass.

Pore width is of interest for the particle usability as a pSLB substrate for protein–silica intercalation. Pore distributions as calculated from N_2 adsorption isotherms using the BJH method are presented in Figure 6B. MPS-3 and MPS-5 showed narrow pore size distributions as well as narrow pore widths, which is in good agreement with TEM and SEM data. MPS-1 and MPS-4 showed wide pore distributions and larger pore widths compared to MPS-3 and MPS-5. Particularly MPS-1 did to a large extent consist of pores in the range of ~6–14 nm, which is a promising characteristic for protein–silica intercalation purposes.

Table 2. Material properties of mesoporous silica particles analyzed by N_2 physisorption.

Material	BET surface area (m^2/g)	Total pore volume (cm^3/g)
MPS-1	493	1.42
MPS-3	769	1.38
MPS-4	650	2.27
MPS-5	737	1.18

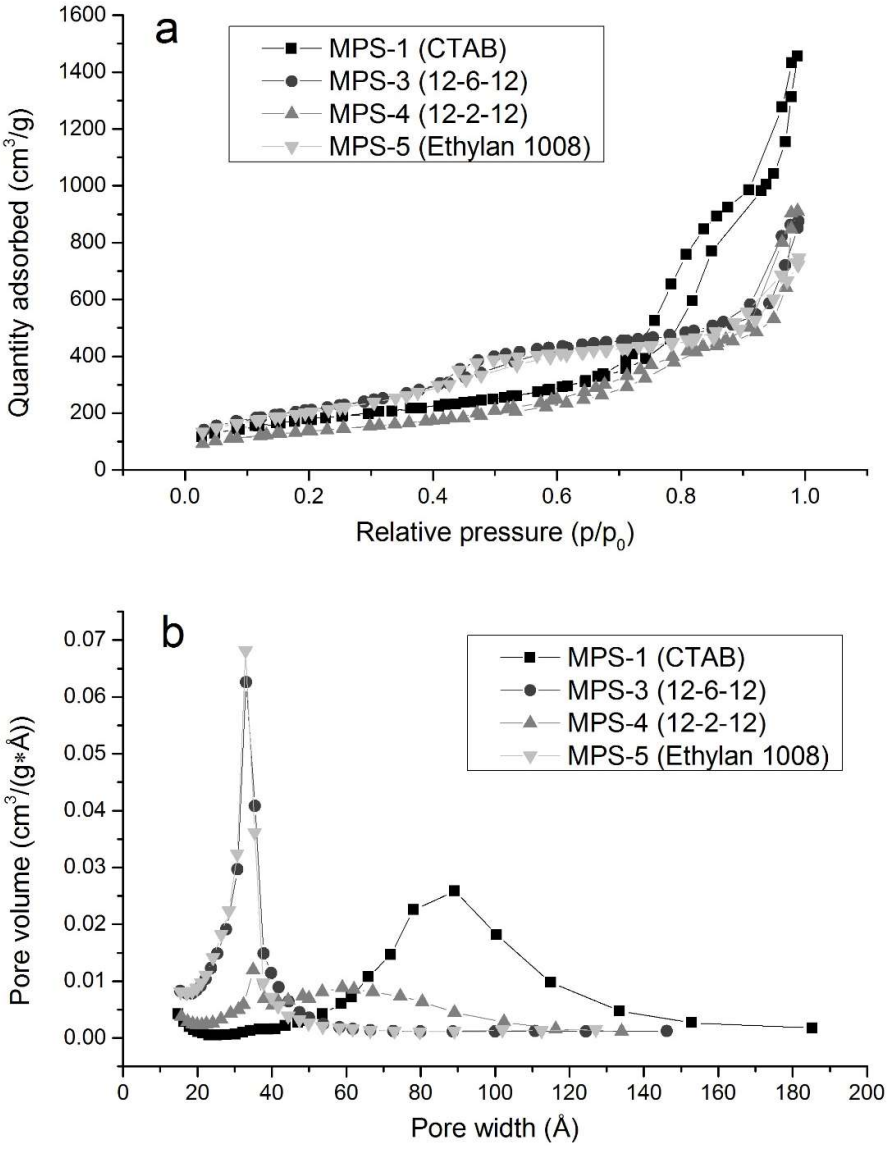

Figure 6. Nitrogen physisorption measurements. (a) Nitrogen adsorption–desorption isotherms and (b) the pore size distribution of the mesoporous nanoparticles.

Since MPS-1 showed greatest potential as a pSLB support, the internal structure of those particles was studied as well. SEM mainly provided data on the particle surface whereas TEM provided data on the particle as a whole, including the surface. In order to specifically assess the internal pore structure of MPS-1, particles were embedded in epoxy plastic and cut into thin (~60 nm) slices. These slices were studied in TEM (Figure 7) and the MPS-1 particle interior was concluded to show great similarity to intact MPS-1 particles studied using TEM (Figure 5A). This observation strengthened the claim that these particles obtained their pore morphology from certain characteristics of the W/O/W emulsion, which was proposed to give rise to the pore structure.

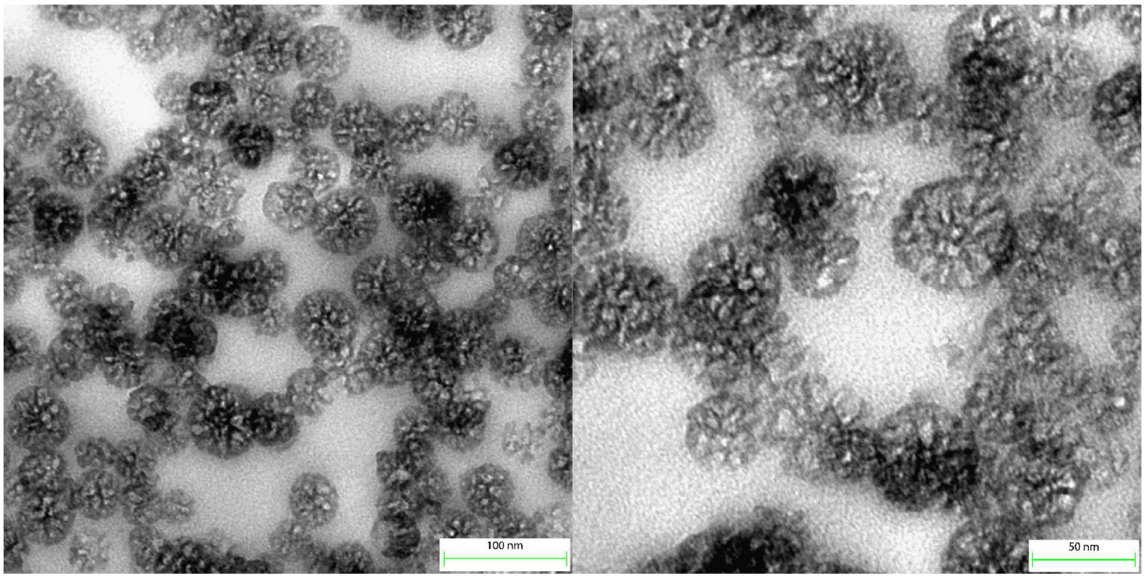

Figure 7. TEM micrographs of MPS-1 particles embedded in epoxy plastic and cut into thin (~60 nm) slices.

4.3 Proteoliposomes

The size, morphology, and water transport capability of proteoliposomes were assessed prior to deposition on the mesoporous silica substrate (Figure 8). Cryo-TEM was used to study the morphology of the proteoliposomes since it is not possible to study liquids in the ultra-high vacuum conditions of a regular TEM. The micrographs depicting liposomes (proteoliposomes without proteins) (Figure 8A) and proteoliposomes (Figure 8B) showed clear and interesting differences. The first observation was that the bilayer thicknesses among liposomes seemed more uniform than the bilayer thicknesses among proteoliposomes. Assessing the bilayer thicknesses of 30 liposomes and 30 proteoliposomes from cryo-TEM micrographs confirmed that there were differences in bilayer thickness between liposomes (Figure 8C) and proteoliposomes (Figure 8D). Interestingly, the liposomes consisted of a single bilayer thickness population centered around 5 nm whereas the proteoliposomes consisted of two populations centered around 5 and 7 nm, respectively. This observation was attributed to preferential protein insertion in the reconstitution process, favoring some liposomes over others. In connection to this it was also observed that the proteoliposomes having a bilayer thickness of 7 nm never were closer than 1.9 nm to any other liposome. This strengthened the reasoning that there were both liposomes and proteoliposomes present in the proteoliposome sample since extracellular domains of hAQP4 would protrude from the bilayer and provide a sterical barrier in between the proteoliposome and its neighbor.

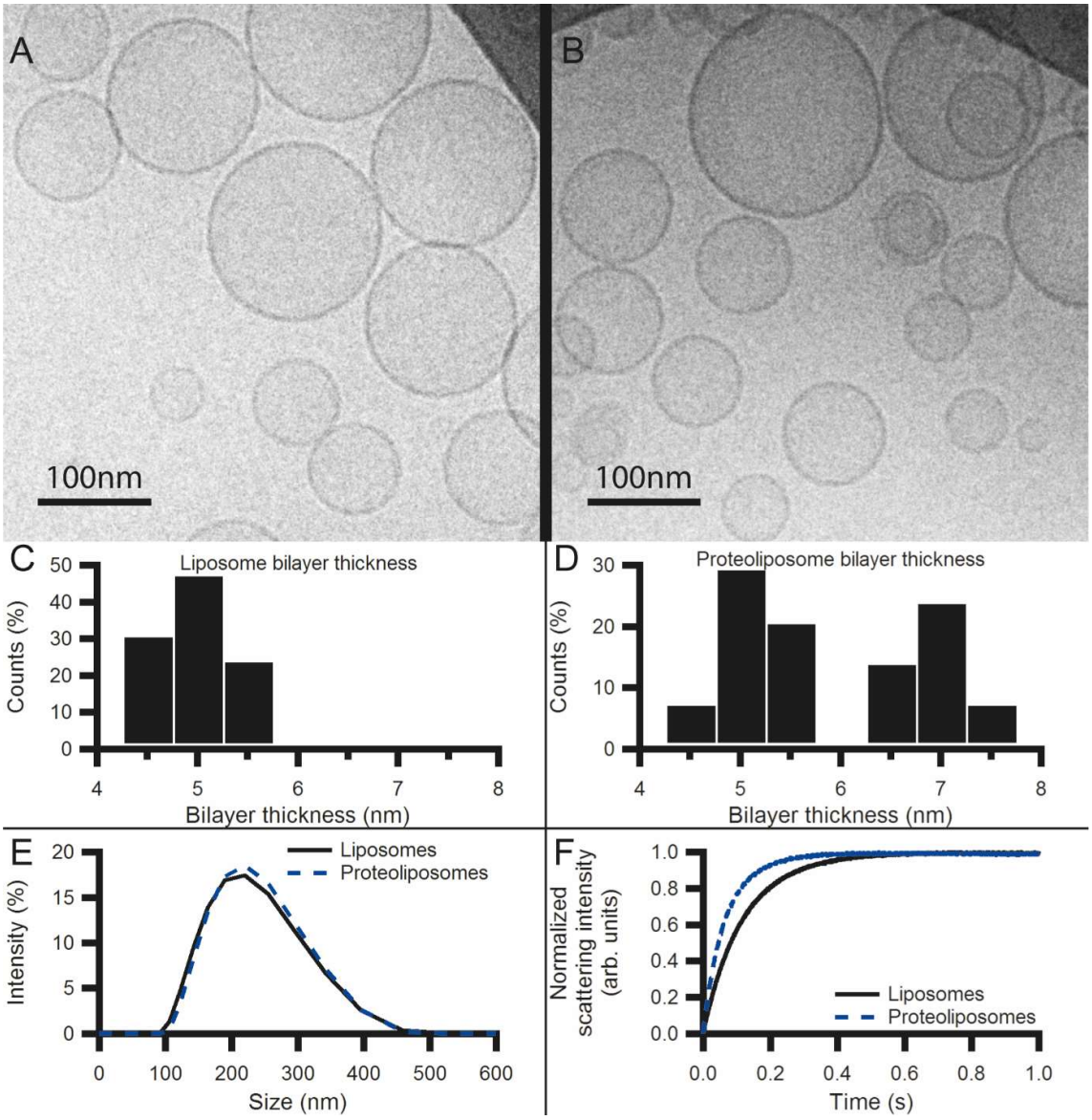

Figure 8. (A) Cryo-TEM micrograph of a POPC liposome sample. (B) Cryo-TEM micrograph of an hAQP4-containing POPC proteoliposome sample. (C) Bilayer thickness distribution of 30 liposomes as determined from POPC liposome samples showing one population centered at 5 nm. (D) Bilayer thickness distribution of 30 proteoliposomes as determined from hAQP4-containing POPC proteoliposome samples showing two populations centered at 5 and 7 nm, respectively. (E) Size distribution of a POPC liposome sample (solid) and an hAQP4-containing POPC proteoliposome sample (dashed) as assessed by DLS. (F) hAQP4 functionality assessment through stopped-flow light scattering measurements. hAQP4-containing POPC proteoliposomes (dashed) show 3 times higher osmotic water permeability than that of POPC liposomes (solid).

The size distributions of liposomes and proteoliposomes were assessed by DLS (Figure 8E). Liposomes and proteoliposomes showed very similar size distributions of 227 ± 9 nm and 234 ± 11 nm, respectively.

Proteoliposomes showed 3 times higher water transport rate compared to liposomes as assessed by stopped-flow light scattering, with osmotic water permeability values of 150.2 ± 1.0 μm s^{-1} and 55.6 ± 0.3 μm s^{-1}, respectively (Figure 8F). This is in accordance with previously reported observations,[40] and therefore a confirmation that the proteins are functional after having been subjected to the reconstitution process.

4.4 Protein-containing supported lipid bilayers

The formation process and characteristics of the pSLB were studied to confirm that a pSLB was obtained and to assess under which circumstances it was formed. The time-resolved analysis methods QCM-D and TIRF microscopy were used to assess the pSLB formation process. QCM-D showed that pSLB formation was readily conducted on mesoporous silica, albeit requiring approximately one order of magnitude more time compared to SLB formation on the same substrate (Figure 9A). Proteoliposomes were also introduced to a nonporous silica substrate, whereby no pSLB formation was observed using QCM-D.

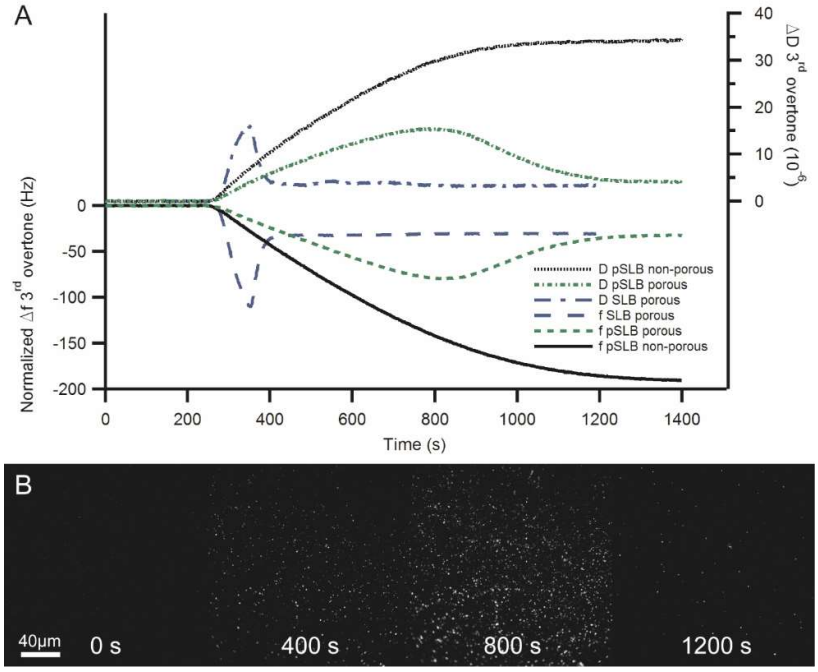

Figure 9. (A) QCM-D recording of the bilayer formation process from POPC liposomes and hAQP4-containing POPC proteoliposomes on nonporous and mesoporous silica, where sample was continuously added to the sensors at a flow rate of 50 μL min^{-1}. Normalized frequency shift on the left axis and dissipation on the right axis are presented as a function of time. Positive values represent ΔD and negative values represent Δf for the supported lipid bilayer (SLB) formation on mesoporous silica (blue), protein-containing supported lipid bilayer (pSLB) formation on nonporous silica (black), and pSLB formation on mesoporous silica (green). (B) TIRF microscopy images showing the pSLB formation on mesoporous silica as a function of time; 800 s of intact vesicle adsorption is seen as an increasing amount of bright dots (fluorescently labeled proteoliposomes), which is followed by proteoliposome rupture, pSLB formation, and hence rapid diffusion of fluorophores in the bilayer.

The pSLB formation process was also investigated using TIRF microscopy (Figure 9B), which confirmed pSLB formation on mesoporous silica. Furthermore, lipid and hAQP4 diffusivity measurements were conducted using FRAP once the pSLB had been formed. The pSLB lipid diffusivity was 2.42 ± 0.04 $\mu m^2 s^{-1}$, which was slightly higher than the pSLB lipid diffusivity on nonporous silica (2.21 ± 0.07 $\mu m^2 s^{-1}$). hAQP4 was immobile on mesoporous silica, which could possibly be due to pore utilization. AQP4 has previously been shown to be immobile when forming orthogonal arrays in native cell membranes, [41] which could possibly be the case in our setup as well.

The formed pSLB was further studied using neutron reflectivity to assess the positioning of hAQP4 in the proposed water filter design. The reflectivity profiles of pSLBs on nonporous silicon oxide (Figure 10A) and mesoporous silica (Figure 10B) show the existence of bilayers on both substrates. The Bragg peak that appeared in the reflectivity profile on mesoporous silica was due to the long-range ordering of the pore network, as was previously seen using SAXS (Figure 3B).

The bilayers formed on nonporous and mesoporous substrates did, however, share few common characteristics. The bilayer formed on the nonporous substrate did not seem to contain any proteins, as can be seen from Figures 10C and D. The bilayer formed on the nonporous substrate hence consisted of POPC only. The best fit to the data was obtained by including additional bilayer stacks on top of the bilayer, representing the existence of coadsorbed proteoliposomes. The bilayer surface coverage was 95 ± 5 % and the coadsorbed vesicle coverage was 3 %.

The bilayer formed on the mesoporous silica substrate was completely different, as can be seen in Figures 10E and F. The bilayer surface coverage was similar at 87 ± 5 % but the hAQP4 content in the bilayer was as high as 58 ± 5 %. There were no coadsorbed vesicles resting on top of the pSLB. The greatest benefit of using neutron reflectivity is its high resolution in the z-direction (Å), meaning that differences in material composition in the direction perpendicular to the surface can accurately be probed. The plot of volume fraction as a function of distance from the center of the bilayer for the pSLB on mesoporous silica showed that the extracellular domains of the protein extended 10.0 ± 1.0 nm into the bulk solution. What was even more exciting was that proteins oriented in the opposite direction, having extracellular domains facing the substrate, were shown to reach 7.2 ± 1.0 nm into the substrate. As much as 10 ± 5 % of the volume at that depth was occupied by protein, suggesting that the proteins make use of the water-filled pores in the porous silica to accommodate their extracellular domains.

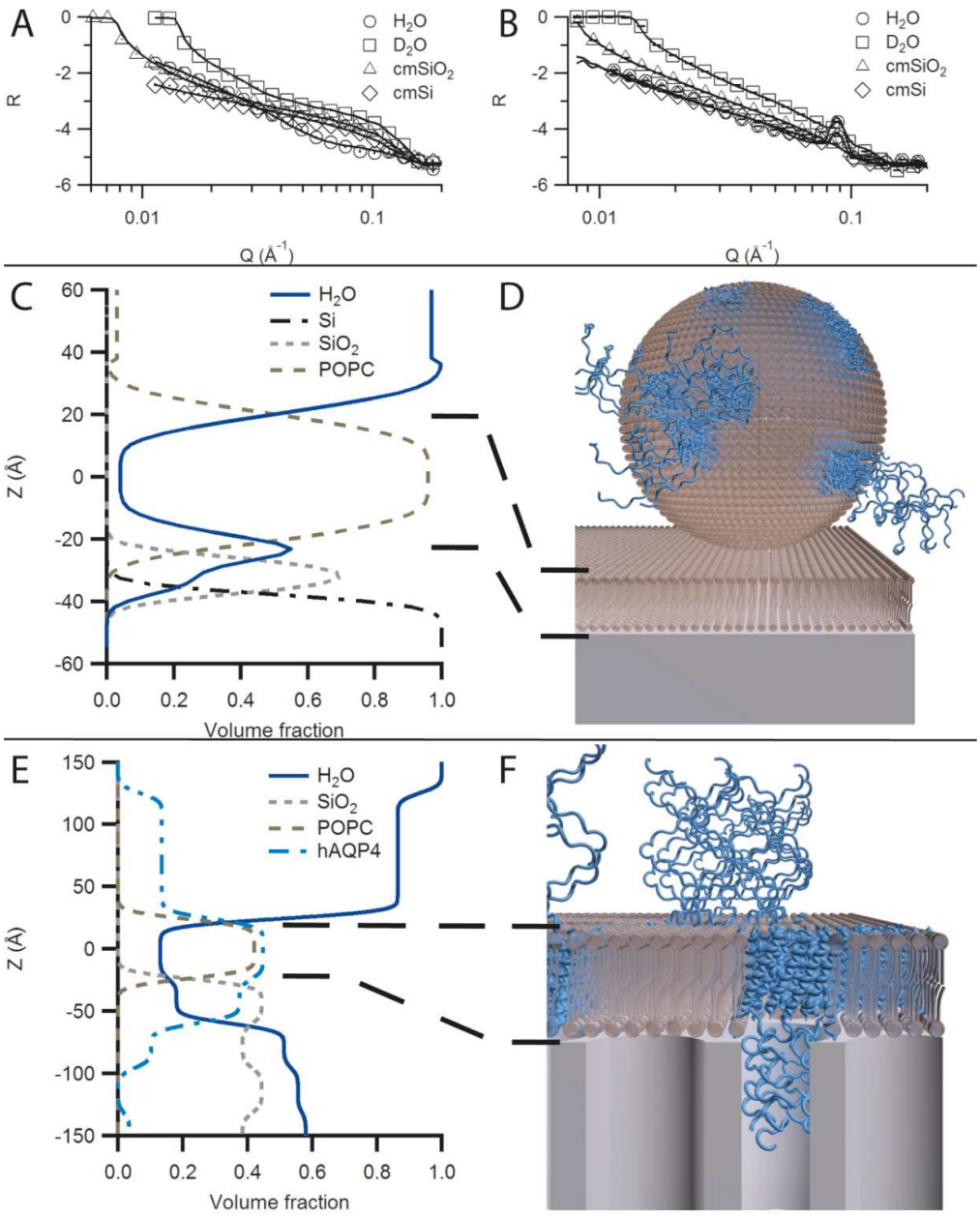

Figure 10. (A) NR curves and best fits (lines) for a supported lipid bilayer (SLB) on a nonporous substrate measured in four different bulk contrasts: H_2O (circles), D_2O (squares), $cmSiO_2$ (triangles), and cmSi (diamonds). (B) NR curves and best fits (lines) for a protein-containing supported lipid bilayer (pSLB) on a mesoporous substrate, measured in the same four contrasts as the SLB. A Bragg peak is visible due to the long-range pore order in the silica substrate. (C) Volume fractions corresponding to the fits for the SLB on a nonporous Si substrate (bilayer thickness = 4.6 nm). (D) Illustration visualizing the NR data for the POPC (brown) bilayer on nonporous silica (gray) with an hAQP4 (blue) containing proteoliposome coadsorbed on top of the bilayer. (E) Volume fractions corresponding to the fits to the Si crystal surface for the pSLB on a mesoporous substrate (bilayer thickness = 4.8 nm). hAQP4 protruded 7.2 ± 1.0 nm into the porous substrate and 10.0 ± 1.0 nm into the bulk when facing the substrate and away from the substrate, respectively. (F) Illustration visualizing the NR data for the POPC (brown) bilayer containing hAQP4 (blue) intercalated with mesoporous silica (gray).

5 Concluding remarks and Future work

Access to clean drinking water is a prerequisite for a healthy life. More than half a billion people do not have access to an improved source of drinking water, meaning that they are exposed to water-borne infections and other diseases on a regular basis. Global warming and increasing pollution add more stress to societies that are already suffering from a lack of safe drinking water.

The sea is one source of water that has drawn a lot of interest lately. Desalination through RO is a commonly used procedure to convert saline sea water into drinking water. It is, however, an energy demanding filtration process that almost exclusively is conducted in large scale desalination plants. Since approximately 70 % of the Earth's surface is covered in water, sea water is an abundant source of water. More energy efficient ways of converting saline water into drinking water are needed in order to approach a sustainable future.

Nature is a master of water desalination using a variety of processes conducted on different length scales. The aim of this thesis was to come one step closer to energy efficient and low-cost water desalination for drinking water production by mimicking nature. The approach was to develop a design that mimics the water transport across the cell membrane. The ultimate goal of the project is to be able to utilize this kind of design as a filter in water treatment processes in the future.

This thesis presented the design of a proposed biomimetic water filter along with the additional design option of using custom designed mesoporous silica nanoparticles instead of a mesoporous silica thin film as the substrate supporting the pSLB. The design was thoroughly characterized, providing knowledge on the morphology and dimensions of the mesoporous silica thin film and mesoporous silica nanoparticles as well as the proteoliposomes. The most important contribution of this thesis is however the study of the interface between the protein-containing supported lipid bilayer and mesoporous silica thin film. Aquaporins were shown to utilize the aqueous volume underneath the bilayer provided by the pores, resulting in protein–silica intercalation. This is an interesting feature in reverse osmosis desalination processes since high pressures are usually required to overcome the osmotic pressure that builds up across the filter membrane in the process. Good intercalation and the possibility for proteins to protect their extracellular domains within the pores are likely beneficial characteristics of a biomimetic water treatment filter.

What is not yet achieved in the project is to use the proposed filter design described in this thesis for drinking water production. The next step in the process of development will be to find suitable methods for evaluating the water treatment performance of such a filter. Other efforts within the project are focused on reinforcing the proposed filter design further to make the chances of implementation in pressure-driven processes even higher. The ultimate goal of the project is to achieve energy-efficient and low-cost water treatment using biomimicry. This thesis is a step in the right direction but there is still a lot more to be discovered, developed and finally implemented.

Acknowledgements

I would like to start by acknowledging the Swedish Research Council FORMAS for providing the funding to make this project happen.

I am very grateful to my main supervisor Martin Andersson for putting a lot of interest and passion into my project. I am privileged to have such an engaged, knowledgeable and caring supervisor that never runs out of ideas and fun things to try out. I will likely never stop to be amazed of how easy you come up with solutions, but I am trying to mimic that as well.

I am also grateful to my assistant supervisor Fredrik Höök. I am equally impressed every time you perform a back-of-the-envelope calculation. Thank you for engaging in the project and particularly for providing lots of valuable feedback on the paper.

I would like to thank the present and former members of M.A. Research for being such a cheerful group of people that provide me with a great working environment. In particular, I would like to thank my office mate Emma, my predecessor Maria Wallin, and my former diploma worker Maria Japlin for making work much more fun and easy. Chlor, Johan, Anand, Saba, Ali, Mats, Maria Pihl, Gustav, Andy, and diploma workers, you are all great!

Co-authors, collaborators, and instrument scientists are acknowledged for giving me a pleasant experience of how smooth and rewarding collaborations can be. A special thanks to Krister Holmberg and Hanna Gustafsson for giving me the opportunity to work on silica particles and with Hanna in further collaborations. Most importantly, I am also grateful to Hanna for spreading a positive atmosphere. Continue to do so in Australia as well!

The people at the Divisions of Applied Chemistry and Biological physics are welcoming and fun, which contributes to an awesome working environment. I would like to thank Åsa Östlund and Lars Nordstierna for inviting me to TYK as well as Jonatan and Alex for taking great care of me from the beginning and ever since, both at and outside work. I would also like to thank Hudson and Mokhtar for all the practical assistance and beneficial discussions.

My fellow members of the Chemistry and Chemical Engineering & Biology and Biological Engineering joint PhD student council are acknowledged for being passionate about improving our working environment and for providing me with fika now and then.

Innebandy is one of the best ways of improving the working environment and I would like to thank all of you that have joined me in countless hours of chasing a ball and having pizza!

Last but definitely not least I would like to thank my family and non-Chalmers friends for providing me with all sorts of wonderful reasons not to work all the time. A special mention, however, goes to the group of childhood friends who still believe that I will cure cancer one day, maybe those thoughts made me what I am today. Massive thanks to my family for all the support throughout the years and for making sure that I am still going strong. Very last but also very not least, I would like to thank my lovely wife Malin who is always there to make me feel appreciated and loved. I appreciate all the ideas on activities you come up with and I hope that our kid will possess the same joy and energy as you do!

References

1. *Progress on Drinking Water and Sanitation: 2015 update*; WHO, UNICEF, 2015.
2. *Progress on Drinking Water and Sanitation: 2012 update*; WHO, UNICEF, 2012.
3. *Progress on Drinking Water and Sanitation: 2014 update*; WHO, UNICEF, 2014.
4. Cook, J.; Oreskes, N.; Doran, P. T.; Anderegg, W. R. L.; Verheggen, B.; Maibach, E. W.; Carlton, J. S.; Lewandowsky, S.; Skuce, A. G.; Green, S. A.; Nuccitelli, D.; Jacobs, P.; Richardson, M.; Winkler, B.; Painting, R.; Rice, K. *Environ. Res. Lett.* **2016,** 11, (4), 7.
5. Rahmstorf, S.; Box, J. E.; Feulner, G.; Mann, M. E.; Robinson, A.; Rutherford, S.; Schaffernicht, E. J. *Nat. Clim. Chang.* **2015,** 5, (5), 475-480.
6. Cole, M.; Lindeque, P.; Halsband, C.; Galloway, T. S. *Mar. Pollut. Bull.* **2011,** 62, (12), 2588-2597.
7. Stackelberg, P. E.; Furlong, E. T.; Meyer, M. T.; Zaugg, S. D.; Henderson, A. K.; Reissman, D. B. *Sci. Total Environ.* **2004,** 329, (1-3), 99-113.
8. Werber, J. R.; Osuji, C. O.; Elimelech, M. *Nat. Rev. Mater.* **2016,** 1, (5), 16.
9. Geise, G. M.; Paul, D. R.; Freeman, B. D. *Prog. Polym. Sci.* **2014,** 39, (1), 1-42.
10. Huisman, L.; Wood, W. E. *Slow sand filtration*; WHO, 1974.
11. Bhushan, B. *Philos. Trans. R. Soc. A-Math. Phys. Eng. Sci.* **2009,** 367, (1893), 1445-1486.
12. Caroni, P.; Zurini, M.; Clark, A.; Carafoli, E. *J. Biol. Chem.* **1983,** 258, (12), 7305-7310.
13. Breitwieser, G. E.; Szabo, G. *J. Gen. Physiol.* **1988,** 91, (4), 469-493.
14. Preston, G. M.; Carroll, T. P.; Guggino, W. B.; Agre, P. *Science* **1992,** 256, (5055), 385-387.
15. Yang, B. X.; Verkman, A. S. *J. Biol. Chem.* **1997,** 272, (26), 16140-16146.
16. Denker, B. M.; Smith, B. L.; Kuhajda, F. P.; Agre, P. *J. Biol. Chem.* **1988,** 263, (30), 15634-15642.
17. King, L. S.; Kozono, D.; Agre, P. *Nat. Rev. Mol. Cell Biol.* **2004,** 5, (9), 687-698.
18. Ho, J. D.; Yeh, R.; Sandstrom, A.; Chorny, I.; Harries, W. E. C.; Robbins, R. A.; Miercke, L. J. W.; Stroud, R. M. *Proc. Natl. Acad. Sci. U. S. A.* **2009,** 106, (18), 7437-7442.
19. Lu, M. Q.; Lee, M. D.; Smith, B. L.; Jung, J. S.; Agre, P.; Verdijk, M. A. J.; Merkx, G.; Rijs, J. P. L.; Deen, P. M. T. *Proc. Natl. Acad. Sci. U. S. A.* **1996,** 93, (20), 10908-10912.
20. Hasegawa, H.; Ma, T. H.; Skach, W.; Matthay, M. A.; Verkman, A. S. *J. Biol. Chem.* **1994,** 269, (8), 5497-5500.
21. Furman, C. S.; Gorelick-Feldman, D. A.; Davidson, K. G. V.; Yasumura, T.; Neely, J. D.; Agre, P.; Rash, J. E. *Proc. Natl. Acad. Sci. U. S. A.* **2003,** 100, (23), 13609-13614.
22. van Meer, G.; Voelker, D. R.; Feigenson, G. W. *Nat. Rev. Mol. Cell Biol.* **2008,** 9, (2), 112-124.
23. Koynova, R.; Caffrey, M. *Biochim. Biophys. Acta-Rev. Biomembr.* **1998,** 1376, (1), 91-145.
24. Stober, W.; Fink, A.; Bohn, E. *J. Colloid Interface Sci.* **1968,** 26, (1), 62-69.
25. Soler-illia, G. J. D.; Sanchez, C.; Lebeau, B.; Patarin, J. *Chem. Rev.* **2002,** 102, (11), 4093-4138.
26. Wan, Y.; Zhao, D. Y. *Chem. Rev.* **2007,** 107, (7), 2821-2860.

27. Beck, J. S.; Vartuli, J. C.; Roth, W. J.; Leonowicz, M. E.; Kresge, C. T.; Schmitt, K. D.; Chu, C. T. W.; Olson, D. H.; Sheppard, E. W.; McCullen, S. B.; Higgins, J. B.; Schlenker, J. L. *J. Am. Chem. Soc.* **1992,** 114, (27), 10834-10843.
28. Zhao, D. Y.; Feng, J. L.; Huo, Q. S.; Melosh, N.; Fredrickson, G. H.; Chmelka, B. F.; Stucky, G. D. *Science* **1998,** 279, (5350), 548-552.
29. Brinker, C. J.; Lu, Y. F.; Sellinger, A.; Fan, H. Y. *Adv. Mater.* **1999,** 11, (7), 579-585.
30. Nandiyanto, A. B. D.; Kim, S. G.; Iskandar, F.; Okuyama, K. *Microporous Mesoporous Mat.* **2009,** 120, (3), 447-453.
31. Brunauer, S.; Emmett, P. H.; Teller, E. *J. Am. Chem. Soc.* **1938,** 60, 309-319.
32. Barrett, E. P.; Joyner, L. G.; Halenda, P. P. *J. Am. Chem. Soc.* **1951,** 73, (1), 373-380.
33. Finsy, R. *Adv. Colloid Interface Sci.* **1994,** 52, 79-143.
34. Van Heeswijk, M. P. E.; Van Os, C. H. *J. Membr. Biol.* **1986,** 92, (2), 183-193.
35. Thompson, N. L.; Pearce, K. H.; Hsieh, H. V. *Eur. Biophys. J. Biophys. Lett.* **1993,** 22, (5), 367-378.
36. Poo, M. M.; Cone, R. A. *Nature* **1974,** 247, (5441), 438-441.
37. Liebman, P. A.; Entine, G. *Science* **1974,** 185, (4149), 457-459.
38. Bucknall, D. G.; Penfold, J.; Webster, J. R. P.; Zarbakhsh, A.; Richardson, R. M.; Rennie, A.; Higgins, J. S.; Jones, R. A. L.; Thomas, R. K.; Roser, S.; Dickinson, E. In *SURF - a second generation neutron reflectometer*, Proceedings of the meetings ICANS-XIII and ESS-PM4 Volume I, Switzerland, 1995; Paul Scherrer Institut: Switzerland, p 440.
39. Sing, K. S. W.; Everett, D. H.; Haul, R. A. W.; Moscou, L.; Pierotti, R. A.; Rouquerol, J.; Siemieniewska, T. *Pure Appl. Chem.* **1985,** 57, (4), 603-619.
40. Oberg, F.; Sjohamn, J.; Conner, M. T.; Bill, R. M.; Hedfalk, K. *Mol. Membr. Biol.* **2011,** 28, (6), 398-411.
41. Crane, J. M.; Verkman, A. S. *J. Cell Sci.* **2009,** 122, (6), 813-821.